Available online at www.sciencedirect.com
ScienceDirect
Medical Engineering & Physics 30 (2008) 680–686
Medical Engineering & Physics
www.elsevier.com/locate/medengphy

MicroPET reconstruction with random coincidence correction via a joint Poisson model

Tai-Been Chen [a], Jyh-Cheng Chen [c,e], Henry Horng-Shing Lu [b,*], Ren-Shyan Liu [d]

[a] *Department of Medical Imaging and Radiological Sciences, I-Shou University, Taiwan, ROC*
[b] *Institute of Statistics, National Chiao Tung University, 1001 Ta Hsueh Road, Hsinchu 30050, Taiwan, ROC*
[c] *Department of Biomedical Imaging and Radiological Sciences, National Yang-Ming University, Taiwan, ROC*
[d] *School of Medicine, National Yang-Ming University, Taiwan, ROC*
[e] *Department of Education and Research, Taipei City Hospital, Taiwan, ROC*

Received 27 March 2006; received in revised form 19 May 2007; accepted 23 May 2007

Abstract

Positron emission tomography (PET) can provide *in vivo*, quantitative and functional information for diagnosis; however, PET image quality depends highly on a reconstruction algorithm. Iterative algorithms, such as the maximum likelihood expectation maximization (MLEM) algorithm, are rapidly becoming the standards for image reconstruction in emission-computed tomography. The conventional MLEM algorithm utilized the Poisson model in its system matrix, which is no longer valid for delay-subtraction of randomly corrected data. The aim of this study is to overcome this problem. The maximum likelihood estimation using the expectation maximum algorithm (MLE-EM) is adopted and modified to reconstruct microPET images using random correction from joint prompt and delay sinograms; this reconstruction method is called PDEM. The proposed joint Poisson model preserves Poisson properties without increasing the variance (noise) associated with random correction. The work here is an initial application/demonstration without applied normalization, scattering, attenuation, and arc correction. The coefficients of variation (CV) and full width at half-maximum (FWHM) values were utilized to compare the quality of reconstructed microPET images of physical phantoms acquired by filtered backprojection (FBP), ordered subsets-expected maximum (OSEM) and PDEM approaches. Experimental and simulated results demonstrate that the proposed PDEM produces better image quality than the FBP and OSEM approaches.

PACS: 87.59.Vb; 87.59.Qx; 87.59.Sz; 87.59.−e

Keywords: MLE-EM; FBP; OSEM; PDEM; FORE; CV; FWHM

1. Introduction

The high spatial resolution and sensitivity of microPET make it an ideal modality for *in vivo* gene imaging. Those images can be employed to monitor the effects of gene therapy inside animal bodies. High-quality image reconstruction is important when establishing a solid basis for quantitative study of microPET images [1,2].

The maximum likelihood estimation with expectation-maximization (MLE-EM) algorithms has been utilized to reconstruct emission-computed tomography [3,4]. Statistical analysis that supports positron emission tomography (PET) has been discussed elsewhere [5]. The MLE-EM technique can model randomness in emission tomography with the asymptotic efficiency of MLE by applying the row operation and monotonic convergence using the EM algorithm. Furthermore, the EM algorithm can be parallelizable for 3D PET image reconstruction [6].

The generation of quantitative PET images requires that the effects of random coincidences and coincidence efficiency are corrected [7,8]. One random correction approach applies single count rates to a prompt sinogram [9]. This approach is generally based on geometrical and physical characteristics. However, this approach makes many assumptions for approximations that can decrease the accuracy of random

* Corresponding author. Tel.: +886 3 5731870; fax: +886 3 5728745.
E-mail address: hslu@stat.nctu.edu.tw (H.H.-S. Lu).

1350-4533/$ – see front matter © 2007 IPEM. Published by Elsevier Ltd. All rights reserved.
doi:10.1016/j.medengphy.2007.05.013

correction below that obtained using methods that utilize both prompt and delay sinograms. An alternative approach applies random pre-correction to sinograms by subtracting the delay sinogram from a prompt sinogram before processing of images reconstruction. The random pre-correction using various approximations has been applied to correct accidental (or random) coincidental events [10,11]. Novel methods have been developed to approximate random pre-correction [12–14]. However, random pre-correction increases variance (noise) [13,15]. Since the distribution of random pre-correction is no longer Poisson-distributed, the shifted Poisson methods and saddle-point (SD) approximation have been generated to enhance approximation in [16]. This study proposes a joint Poisson model with MLE-EM reconstruction and random correction to prompt and delay sinograms without using approximations or increasing variance.

Simulations, physical phantoms and real mouse studies of the proposed reconstruction method using the microPET R4 system were performed. This study considered analyzed and assessed reconstruction of 2D data obtained from 3D sinograms after applying the Fourier rebinning (FORE) method [17] to verify the proposed approach. The proposed technique can also be utilized by future studies reconstructing 3D images.

2. Methodology

Two independent Poisson models associated with prompt and delay sinograms are labeled (1) and (2).

$$n_{\mathrm{p}}^{*}(d) \sim \mathrm{Poisson}(\lambda^{*}(d)), \tag{1}$$

$$n_{\mathrm{d}}^{*}(d) \sim \mathrm{Poisson}(\lambda_{\mathrm{r}}^{*}(d)), \tag{2}$$

where $\lambda^{*}(d) = \lambda_{\mathrm{t}}^{*}(d) + \lambda_{\mathrm{r}}^{*}(d) = \sum_{\mathrm{b}} P(b,d)\lambda_{\mathrm{t}}(b) + \lambda_{\mathrm{r}}^{*}(d)$, $b = 1, 2, \ldots, B$, and $d = 1, 2, \ldots, D$.

The term $n_{\mathrm{p}}^{*}(d)$ is the number of coincidental events in the prompt sinogram at the dth projection line of response (LOR), which is formed by two detectors with the Poisson parameter or mean, $\lambda^{*}(d)$; $n_{\mathrm{d}}^{*}(d)$ is the number of random coincidental events in the delay sinogram with the Poisson parameter $\lambda_{\mathrm{r}}^{*}(d)$; $P(b,d)$ is the system probability matrix from the bth pixel to the dth detection tube. Parameters $\lambda_{\mathrm{t}}(b)$ and $\lambda_{\mathrm{r}}^{*}(d)$ are unknown and must be estimated. Parameter $\lambda_{\mathrm{t}}(b)$ represents the intensities of true coincidental events. Appendix (A.3) lists the log-likelihood of observed data in the prompt and delay sinograms. Since the MLE is difficult to determine by maximizing Eqs. (1) and (2) numerically, the EM algorithm is utilized (see Appendix A). Eqs. (3) and (4) are the ith iteration steps of the PDEM.

$$\lambda_{\mathrm{t}}^{i}(b) = \frac{\lambda_{\mathrm{t}}^{i-1}(b)}{\sum_{d=1}^{D} P(b,d)} \sum_{d=1}^{D} \frac{n_{\mathrm{p}}^{*}(d)\, p(b,d)}{\sum_{b'=1}^{B} p(b',d)\lambda_{\mathrm{t}}^{i-1}(b') + \lambda_{\mathrm{r}}^{*i-1}(d)}, \tag{3}$$

$$\lambda_{\mathrm{r}}^{*i}(d) = \frac{1}{2}\left[\frac{n_{\mathrm{p}}^{*}(d)\lambda_{\mathrm{r}}^{*i-1}(d)}{\sum_{b'=1}^{B} p(b',d)\lambda_{\mathrm{t}}^{i-1}(b') + \lambda_{\mathrm{r}}^{*i-1}(d)} + n_{\mathrm{d}}^{*}(d)\right], \tag{4}$$

where $i = 1,2, \ldots I$ is the number of iterations.

The MLE-EM algorithm of joint the prompt and delay sinograms is described as follows and such a scheme is called PDEM reconstruction.

2.1. Algorithm for PDEM reconstruction

1. Set initial parameters using filtered backprojection (FBP), the method of moments (MME) or alternative approach.
2. Update the parameters by applying Eqs. (3) and (4).
3. If $|l_{\mathrm{in}}(\lambda_{\mathrm{t}}^{i-1}(b), \lambda_{\mathrm{r}}^{*i-1}(d)) - l_{\mathrm{in}}(\lambda_{\mathrm{t}}^{i}(b), \lambda_{\mathrm{r}}^{*i}(d))| <$ tolerance, then the iteration is terminated; otherwise, go to step 2 and replace the old parameter values with new values.

This method preserves Poisson properties and corrects bias iteratively. In this study, $P(b,d)$ was computed from LORs and the locations of pixels based on the geometric characteristics of the microPET R4, including number of detectors, image size, field of view (FOV), ring diameter, and number of angular views. The matrix size of one slice is 96×84. There are 96 angular views and 84 LORs for each angular view during image scanning. Furthermore, each $P(b,d)$ can be identified from its detector pairs of LOR and image pixel location. Therefore, the PDEM reconstructs the sinogram after being rebinned by FORE approach in the microPET system.

3. System configurations of microPET R4 and data handling

The phantoms and small animals were injected with F-18 FDG and were scanned by the microPET R4. The microPET R4 system consists of 32 rings with 192 detectors per ring; the images were reconstructed using 128×128 pixels. Transaxial projection bin size was 1.213 mm, and axial slice thickness was 1.2115 mm. Coincidence timing window was set at 6×10^{-9} s. The lower and upper level energy thresholds were 350 and 750 keV, respectively. Span of the data set was 3, and maximum ring difference (MRD) of the data set was 31.

The data handling is described as follows: first, list mode data were histogramed into the 3D data with a span of 3 and MRD of 31, which are sized $2 \times 703 \times 96 \times 84$ (i.e., 2 sinograms (prompt and delay) $\times$ 703 slices $\times$ 96 angular views $\times$ 84 projection lines (LORs)) and stored as floating type data. The second data were obtained using random pre-correction and were sized $1 \times 703 \times 96 \times 84$. These 3D data were rebinned into 2D sinograms using the FORE method with dead time and decay corrections. The attenuation, normalization, scattering, and arc corrections were not

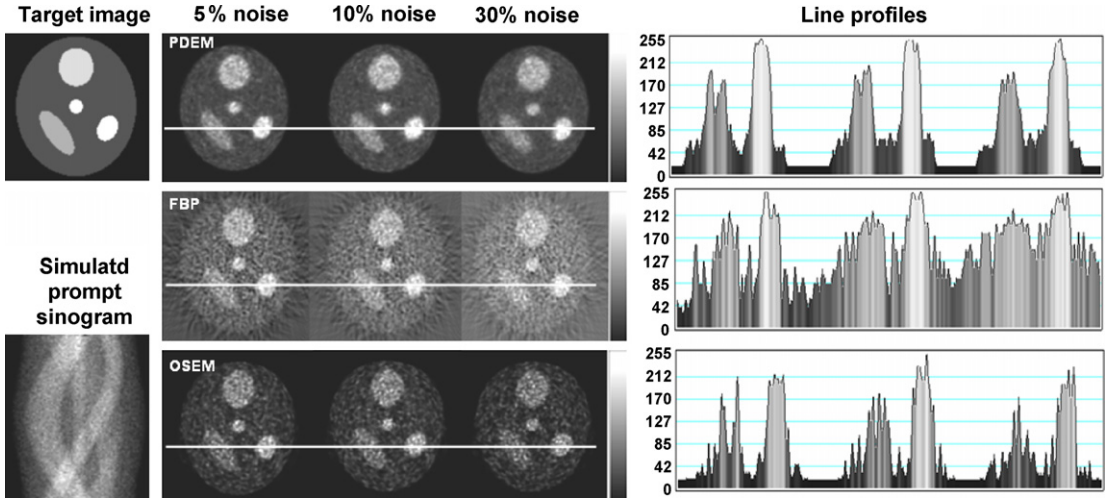

Fig. 1. The modified Shepp-Logan head image was used for simulation studies. The line profiles of PDEM were less noisy than those of FBP and OSEM. The PDEM technique reconstructed better images than did FBP and OSEM with 5%, 10% and 30% random noise. All images were rescaled using their own maximum values.

performed for simplicity as this study only focused on evaluation of random corrections. These further corrections for PDEM reconstruction will need more investigation in future studies.

Two matrices were constructed using the software embedded in microPET R4 (i.e., microPET manager V1.6.4). The first matrix was $2 \times 63 \times 96 \times 84$ (i.e., 2 sinograms (prompt and delay) $\times$ 63 slices $\times$ 96 angular views $\times$ 84 projection lines (LORs)) and stored as floating type data. This matrix was reconstructed using PDEM. The PDEM was compared with the built-in reconstruction schemes, such as 2D FBP and OSEM methods, in the microPET R4 system. The second matrix was obtained using the FORE and on-line random pre-corrected data. The 2D OSEM, using 16 subsets with four iterations, and the 2D FBP were applied to reconstruct the microPET images for comparison with the PDEM results. The default cut-off filter of 0.5 was used with ramp filtering of the 2D FBP. No reconstructed image was smoothed.

4. Simulation, phantom and mouse studies

4.1. Simulation studies

This study utilized a modified Shepp-Logan's head phantom with dimension 128×128 pixels as the simulated object to assess and compare the images reconstructed using PDEM, FORE + FBP, and FORE + OSEM. We assumed that the simulated diameter of a ring was 28.28 mm and FOV diameter was 20 mm. Target image was 128×128 pixels (20 mm $\times$ 20 mm) and rescaled intensity was $\leq$100. For each pixel intensity, $\lambda_t(b)$, was known and then input into $\lambda_t^*(d)$; next, $\lambda_r^*(d)$ is equal to the multiplication of a given noise ratio to $\lambda_t^*(d)$; n_p^* and n_d^* can be simulated using the Poisson distribution with parameters $\lambda_t^*(d)$ and $\lambda_r^*(d)$ as applied to Eqs. (1) and (2). Total counts (sum of prompt and delayed counts) were 276,794, 316,383 and 342,407 with 5%, 10% and 30% noise levels, respectively, for the three slices simulated. The prompt and delayed sinograms had the same matrix

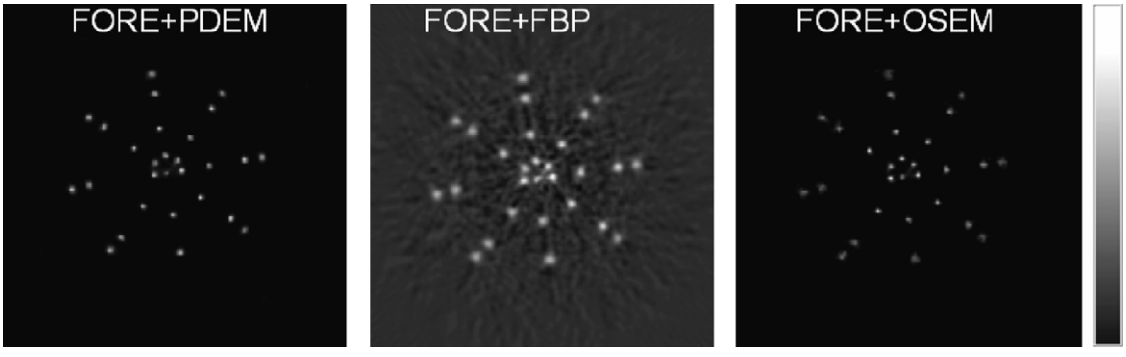

Fig. 2. The 31st slice of the 28 line source phantom reconstructed using the three methods. Both FBP and OSEM are reconstruction methods built into the microPET R4 system. All images were rescaled using their own maximum values.
The images are shown in the rectangular window. Table 1 presents comparisons of their FWHMs.

Table 1
Average and standard deviation (in mm) of 28 FWHMs for horizontal and vertical line profiles measured for comparing the spatial resolutions of PDEM, OSEM and FBP

Methods	Horizontal line profile		Vertical line profile	
	Average	Standard deviation	Average	Standard deviation
PDEM	1.795	0.302	1.775	0.334
OSEM	1.890	0.527	1.863	0.548
FBP	3.641	0.595	3.663	0.624

Those values are measured at the 31st slice. We used line sources in air, thus iterative reconstructions tend to yield narrow point spread images as iteration number increases. Meanwhile, the outer diameter of a line source was 1.27 mm in this study. The FWHM in this table is used to compare the point spread ranges of reconstructed images between PDEM, FBP and OSEM.

size of 96 × 84 (i.e., 96 angular views × 84 projection lines (LORs)) with floating type data. Three random noise ratios of random to true coincidence counts, 5%, 10% and 30% were simulated. The quality of images obtained using the PDEM, FBP and OSEM were compared (Fig. 1). The simulated results demonstrate that the quality of images reconstructed by the PDEM exceeds that of images reconstructed by the FORE + FBP and FORE + OSEM.

4.2. Phantom studies

The first physical phantom was 28 homogenous line sources with an outer diameter of 1.27 mm for each line. This phantom was utilized to assess the performance and accuracy of reconstruction quality between the FBP, OSEM and PDEM (Fig. 2). The spatial resolution was measured using FWHMs from vertical and horizontal line profiles (Table 1). We used linear interpolation to evaluate the profiles of FWHMs. The average and standard deviation of FWHMs in reconstruction images using the PDEM were smaller than those obtained by FBP and OSEM.

Table 2
A circular ROI with a radius of 9 pixels to the center of the uniform phantom was utilized to compare noise levels between PDEM, FBP and OSEM

	PDEM	FBP	OSEM
Average	1146.51	1107.66	1105.36
Standard deviation	36.26	46.82	65.56
Coefficient of variation (%)	3.16	4.23	5.93

Those values were measured at the 40th reconstructed slice.

The second phantom was a uniform cylinder 7.6 cm high with an inner radius of 20 mm; this phantom was utilized to compare image quality obtained using the FBP, OSEM and PDEM. Imaging scan time was 1200 s using the microPET R4 after injection of 276 μCi F-18 FDG. Three reconstruction techniques were applied to reconstruct the 40th slice (Fig. 3). Reconstruction images were presented with the associated central line profiles. Reconstruction images obtaining using the PDEM had better quality than those generated by the FBP and OSEM on their line profiles. A circular region of interest (ROI) was employed to measure the noise level for the different reconstruction methods. The lowest value for coefficient of variation (CV), which is the ratio of standard deviation to mean, was obtained by using the PDEM reconstruction (Table 2).

The PDEM reconstructed better quality images with lower noise levels than the reconstructed approaches built into the

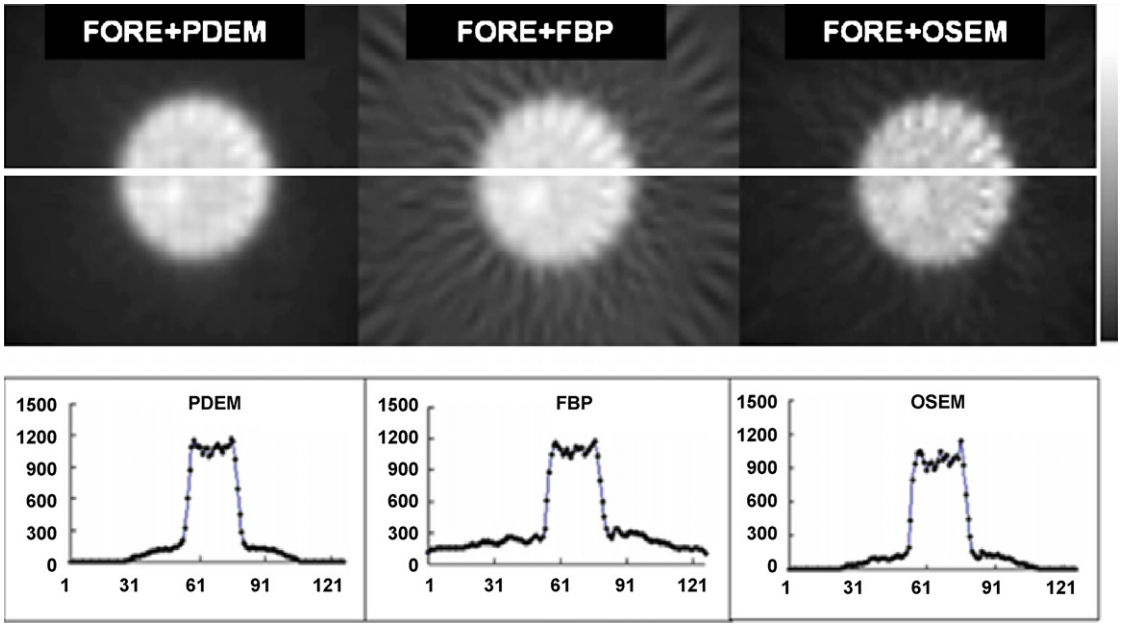

Fig. 3. The reconstructed 40th slice from a uniform phantom was used to investigate noise level generated by the three approaches. The white line indicates the position of the investigated line profile. All images were rescaled using their own maximum values. The images are shown in the rectangular window with enlarged central parts. Table 2 presents comparisons of their CVs.

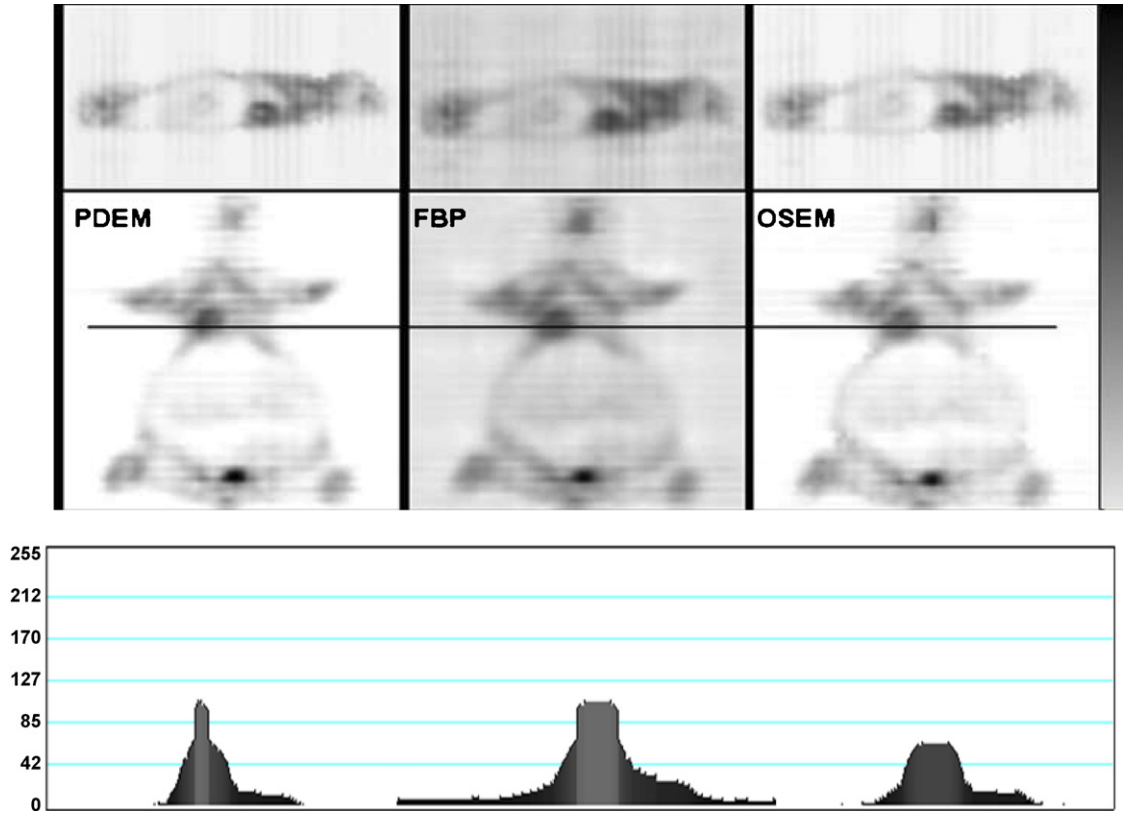

Fig. 4. Coronal and sagittal images of a mouse image reconstructed using PDEM (left), FBP (middle) and OSEM (right). The images reconstructed by PDEM have less noise than those reconstructed by FBP and OSEM, as shown in the respective line profile across the heart. The narrow and high peak demonstrates the contrast of a reconstructed image. The profile of FORE + FBP has an increased bias that demonstrates the quality of image contrast and edge boundary of FORE + FBP is worse. The vertical (top images) and horizontal (middle images) stripes in this figure may be due to rebinning from 3D to 2D, which will need further investigation in future studies. The images are shown in the rectangular window with enlarged central parts.

microPET R4 system during investigations of line and uniform phantoms. Notably, in all reconstruction processing, there was no attenuation, scatter, normalization, or arc correction. However, dead time and decay correction were applied when rebinning 3D sinograms into 2D data.

4.3. Mouse studies

The PDEM method was applied to real data for small mice to compare the quality of reconstructed images with that of images reconstructed using FBP and OSEM. A real normal mice weighed 20 g. Imaging scan time was 600 s using the microPET R4 following an injection of 240.5 μCi F-18 FDG. This mouse was used to perform image quality under a normal amount of F-18 FDG.

All 63 slices after FORE were reconstructed using the PDEM, FBP and OSEM. Fig. 4 presents coronal and sagittal images of a real mouse reconstructed by the PDEM; the absence of normalization on the other hand is obvious in the images (stripe appearance), these images are less noisy and have clearer boundaries than those reconstructed by the FBP and OSEM. Imaging results demonstrate that the PDEM reconstructed images with better contrast and clearer boundaries than those reconstructed with the FBP and OSEM.

5. Discussion

The benefit of the proposed method for PDEM reconstruction is that it retains the characteristics of the Poisson distribution without increasing estimate variance. In physical phantom and real mice studies, the PDEM reconstructed microPET images with higher quality than those reconstructed by methods built into the microPET R4 system, as determined by comparing CVs and FWHMs. Since the microPET R4 scanner supports prompt and delayed coincidences, the PDEM technique can be utilized to reconstruct high-resolution microPET images using random correction, as demonstrated. Although computational cost of the PDEM method is high, increases in computer speed will decrease processing time; relatively faster algorithms can be feasibly developed in future studies. The PDEM method was successfully applied for the microPET reconstruction, this novel method can be utilized in future work to reconstruct clinical PET images based on the same physical principle of data acquisition and mathematical models.

6. Conclusion

This study proposed a novel PDEM method for PET reconstruction using random coincidence correction. The PDEM method reconstructs images with lower CVs and smaller FWHMs than those generated by methods built into microPET R4. The PDEM method has the same benefits as the MLE-EM method in PET reconstruction—namely, row operation, linear complexity, monotonic convergence, non-negativity and parallelizability.

This study investigated the images reconstructed using FORE + PDEM, which was applied to physical phantoms and real mouse data. The noise level, spatial resolutions and boundary of images reconstructed using the FORE + PDEM were better than those generated using the FORE + FBP and FORE + OSEM.

High-contrast, less noisy mouse images with clear object boundaries can be generated using the proposed PDEM method, as demonstrated from real mouse data acquired from the microPET R4 system.

Acknowledgments

The authors would like to thank the National Science Council of the Republic of China, Taiwan, for financially supporting this research under Contract No. NSC 95-3112-B-010-004 and others. Mr. Kuang-Hong Lin is appreciated for his work in acquiring the microPET data. We also thank reviewers for their constructive comments that have improved this study.

Appendix A

Two independent Poisson models associated with prompt and delay sinograms (A.1) and (A.2), are employed.

$$n_{\mathrm{p}}^{*}(d) \sim \mathrm{Poisson}(\lambda^{*}(d)), \tag{A.1}$$

$$n_{\mathrm{d}}^{*}(d) \sim \mathrm{Poisson}(\lambda_{\mathrm{r}}^{*}(d)), \tag{A.2}$$

where $\lambda^{*}(d) = \lambda_{\mathrm{t}}^{*}(d) + \lambda_{\mathrm{r}}^{*}(d) = \sum_{b} P(b,d)\lambda_{\mathrm{t}}(b) + \lambda_{\mathrm{r}}^{*}(d)$, $b = 1, 2, \ldots, B$, and $d = 1, 2, \ldots, D$.

Then, the incomplete log-likelihood of the prompt and delay sinograms are as follows:

$$\begin{aligned} & l_{\mathrm{in}}(\lambda_{\mathrm{t}}(b), \lambda_{\mathrm{r}}^{*}(d)) \\ &= \sum_{d=1}^{D} \left\{ -2\lambda_{\mathrm{r}}^{*}(d) - \sum_{b=1}^{B} P(b,d)\lambda_{\mathrm{t}}(b) + n_{\mathrm{p}}^{*}(d)\ln(\lambda_{\mathrm{r}}^{*}(d) \right. \\ &\quad \left. + \sum_{b=1}^{B} P(b,d)\lambda_{\mathrm{t}}(b)) + n_{\mathrm{d}}^{*}(d)(\ln(\lambda_{\mathrm{r}}^{*}(d)) \right\} \end{aligned} \tag{A.3}$$

First, the observed data, $n_{\mathrm{p}}^{*}(d)$ and $n_{\mathrm{d}}^{*}(d)$ are treated as incomplete data. The EM algorithm uses all data. One possible model of complete data is given by (A.4) and (A.5).

$$n_{\mathrm{p}}^{*}(b,d) \sim \mathrm{Poisson}(p(b,d)\lambda_{\mathrm{t}}(b)), \tag{A.4}$$

$$n_{\mathrm{d}}^{*}(d) \sim \mathrm{Poisson}(\lambda_{\mathrm{r}}^{*}(d)). \tag{A.5}$$

where $n_{\mathrm{p}}^{*}(b,d)$ is the number of emissions at the bth pixel detected by the dth tube; $n_{\mathrm{d}}^{*}(d)$ is the number of random or accidental coincidence (AC) events detected by the dth tube in the delay window; $n_{\mathrm{p}}^{*}(b,d)$ and $n_{\mathrm{d}}^{*}(d)$ are assumed to be statistically independent; $n_{\mathrm{p}}^{*}(d) = \sum_{b=1}^{B} n_{\mathrm{p}}^{*}(b,d) + n_{\mathrm{d}}^{*}(d)$. According to models (A.4) and (A.5), the joint log-likelihood function of PDEM is

$$\begin{aligned} & L(\lambda_{\mathrm{t}}(b), \lambda_{\mathrm{r}}^{*}(d)) \\ &= \sum_{d}\sum_{b} \{n_{\mathrm{p}}^{*}(b,d)\ln(P(b,d)\lambda_{\mathrm{t}}(b)) - P(b,d)\lambda_{\mathrm{t}}(b)\} \\ &\quad + \sum_{d} \{n_{\mathrm{d}}^{*}(d)\ln(\lambda_{\mathrm{r}}^{*}(d)) - \lambda_{\mathrm{r}}^{*}(d)\}. \end{aligned} \tag{A.6}$$

The E-step computes the conditional expectation of the log-likelihood of complete data, given the observed incomplete data and old parameter values; λ_{t}^{0} is initialized by the FBP and $\lambda_{\mathrm{t}}^{*0}$ is initialized by the method of moments, $\bar{n}_{\mathrm{d}}^{*} = \sum_{d} n_{\mathrm{d}}^{*}(d)/D$. This is a function of new parameter values of λ_{t}^{i} and $\lambda_{\mathrm{t}}^{*i}$, where i is the number of iterations, and the formula is given in (A.7).

$$\begin{aligned} & Q(\lambda_{\mathrm{t}}^{i}(b), \lambda_{\mathrm{r}}^{*i}(d) | \lambda_{\mathrm{t}}^{i-1}(b), \lambda_{\mathrm{r}}^{*i-1}(d)) \\ &= E[L(\lambda_{\mathrm{t}}^{i}(b), \lambda_{\mathrm{r}}^{*i}(d))] | n_{\mathrm{p}}^{*}, n_{\mathrm{d}}^{*}, \lambda_{\mathrm{t}}^{i-1}(b), \lambda_{\mathrm{r}}^{*i-1}(d)]. \end{aligned} \tag{A.7}$$

The M-step determines the λ_{t}^{i} and $\lambda_{\mathrm{r}}^{*i}$ values that maximize (A.7), as can be achieved by setting the first derivatives to 0, yielding the solutions given in (A.8) and (A.9).

$$\begin{aligned} \lambda_{\mathrm{t}}^{i}(b) = {} & \frac{\lambda_{\mathrm{t}}^{i-1}(b)}{\sum_{d=1}^{D} P(b,d)} \sum_{d=1}^{D} \\ & \times \frac{n_{\mathrm{p}}^{*}(d)p(b,d)}{\sum_{b'=1}^{B} p(b',d)\lambda_{\mathrm{t}}^{i-1}(b') + \lambda_{\mathrm{r}}^{*i-1}(d)}. \end{aligned} \tag{A.8}$$

$$\lambda_{\mathrm{r}}^{*i}(d) = \frac{1}{2}\left[\frac{n_{\mathrm{p}}^{*}(d)\lambda_{\mathrm{r}}^{*i-1}(d)}{\sum_{b'=1}^{B} p(b',d)\lambda_{\mathrm{t}}^{i-1}(b') + \lambda_{\mathrm{r}}^{*i-1}(d)} + n_{\mathrm{d}}^{*}(d) \right]. \tag{A.9}$$

Conflict of interest

There is no conflict of interest from any financial and personal relationships with other people or organizations that could inappropriately influence (bias) their work.

References

[1] Johnson CA, Seidel J, Carson RE, Gandler WR, Sofer A, Green MV, et al. Evaluation of 3D reconstruction algorithms for a small animal PET camera. IEEE Trans Nucl Sci 1997;44:1303–8.

[2] Chatziioannou A, Qi J, Moore A, Annala A, Nguyen K, Leahy R, et al. Comparison of 3-D maximum *a posteriori* and filtered backprojection algorithms for high-resolution animal imaging with microPET. IEEE Trans Med Imag 2000;19:507–12.

[3] Shepp LA, Vardi Y. Maximum likelihood reconstruction for emission tomography. IEEE Trans Med Imag 1982;MI-1:113–22.

[4] Lange K, Carson RE. EM reconstruction algorithms for emission and transmission tomography. J Comput Assist Tomogr 1984;8:306–16.

[5] Vardi Y, Shepp LA, Kaufman L. A statistical model for positron emission tomography. J Am Stat Assoc 1985;80:8–20.

[6] Chen CM, Lee SY, Cho ZH. Parallelization of the EM algorithm for 3D PET image reconstruction. IEEE Trans Med Imag 1991;10:513–22.

[7] Hoffman EJ, Huang SC, Phelps ME, Kuhl DE. Quantization in positron emission computed tomography: 4. Effect of accidental coincidences. J Comput Assist Tomogr 1981;5:391–400.

[8] Casey ME, Hoffman EJ. Quantization in positron emission computed tomography: 7 a technique to reduce noise in accidental coincidence measurements and coincidence efficiency calibration. J Comput Assist Tomogr 1986;10:845–50.

[9] Rokitta O, Casey M, Wienhard K, Pietrzyk U. Random correction for positron emission tomography using singles count rates. IEEE Nucl Sci Symp Conf Rec 2000;3:1737–40.

[10] Politte DG, Snyder DL. Corrections for accidental coincidences and attenuation in maximum-likelihood image reconstruction for positron-emission tomography. IEEE Trans Med Imag 1991;10:82–9.

[11] Fessler JA, Clinthorne NH, Rogers WL. On complete-data spaces for PET reconstruction algorithms. IEEE Trans Nucl Sci 1993;40:1055–61.

[12] Lu HHS, Tseng WJ. On accelerated cross-reference maximum likelihood estimates for positron emission tomography. In: Conference Record of 1997 IEEE Nuclear Science Symposium, vol. 2. 1997. p. 1484–8.

[13] Lu HHS, Chen CM, Yang IH. Cross-reference weighted least square estimates for positron emission tomography. IEEE Trans Med Imag 1998;17:1–8.

[14] Chen JC, Liu RS, Tu KY, Lu HHS, Chen TB, Chou KL. Iterative image reconstruction with random correction for PET studies. In: Proceedings of the Society of Photo-Optical Instrumentation Engineers, vol. 3979. 2000. p. 1218–29.

[15] Brasse D, Kinahan PE, Lartizien C, Comtat C. Correction methods for random coincidences in 3D whole body PET imaging. In: IEEE Nuclear Science Symposium and Medical Imaging Conference, vol. 4. 2001. p. 2080–4.

[16] Yavuz M, Fessler JA. New statistical models for random pre-corrected PET scans. In: Duncan J, Gindi G, editors. Information processing in medical imaging (lecture notes in computer science), vol. 1230. Springer–Verlag; 1997. p. 190–203.

[17] Michel D, Kinahan PE, Townsend DW, Michel C, Sibomana M, Newport DF. Exact and approximate rebinning algorithms for 3-D PET data. IEEE Trans Med Imag 1997;16:145–58.